ELSEVIER

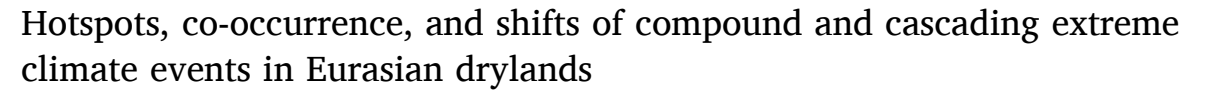
Contents lists available at ScienceDirect

## **Environment International**

journal homepage: www.elsevier.com/locate/envint



## Full length article



Huiqian Yu<sup>a,b</sup>, Nan Lu<sup>a,b,\*</sup>, Bojie Fu<sup>a,b,c</sup>, Lu Zhang<sup>a,b</sup>, Mengyu Wang<sup>a,b</sup>, Hanqin Tian<sup>d</sup>

- a State Key Laboratory of Urban and Regional Ecology, Research Center for Eco-Environmental Sciences, Chinese Academy of Sciences, Beijing 100085, China
- <sup>b</sup> University of Chinese Academy of Sciences, Beijing 100049, China
- <sup>c</sup> Faculty of Geographical Science, Beijing Normal University, Beijing 100875, China
- d Schiller Institute for Integrated Science and Society, Department of Earth and Environmental Sciences, Boston College, Chestnut Hill, MA 02467, USA

## ARTICLE INFO

Handling Editor: Adrian Covaci

Keywords:
Climate extremes
Compound extreme events
Cascading extreme events
Hotspots
ST-DBSCAN
Spatial shifts

## ABSTRACT

Eurasian drylands are the regions that are most vulnerable to climate change. Climate extremes have caused enormous or even devastating impacts on ecosystems and the social economy in this region, and the compound climate extremes (com CEs, two or more extreme events occurring simultaneously) and cascading climate extremes (cas\_CEs, two or more extreme events occurring successively) have exacerbated these problems. However, little is known about the occurrence patterns of com\_CEs and cas\_CEs in the Eurasian drylands. Based on the ERA5 reanalysis data range from 1979 to 2020, we improved the methodology for the extraction of cooccurrence events and identified high-frequency types, their hotspots, and occurrence rhythms (seasonally and annually) in Eurasian drylands. Our results showed that com\_CEs and cas\_CEs have high similarities in the types and spatial hotspots of extreme events; however, the former has a wider geographical and spatial distribution, and the latter has a longer duration. Specifically, co-occurring drought and heatwave events (DH) frequently appear in South Asia and western mid-latitude regions during summer, while in the winter, high latitude regions should be alert to the co-occurrence of drought and low-temperature events (DT). Central Asia and the Mongolian Plateau regions are prone to frequent drought and wind events (DW), and wind and high precipitation events (WP) in the spring and autumn. We have noticed that mid-latitude may suffer from extreme events that have never occurred before, such as com\_DH being scattered sporadically in the first two decades and suddenly surging in West Asia and East Asia after the year 2000, and com\_DT migrating from high-latitude areas such as the Arctic Ocean coast to mid-latitudes. Our results contribute to understanding hotspots of co-occurring CEs in Eurasian drylands, where more efforts will be needed in the future, especially in mid-latitudes which may suffer extreme climate events that have never occurred before.

## 1. Introduction

Extreme weather and climate events (also referred to as climate extremes) have increased in frequency and intensity in recent years (IPCC, 2021). While it is currently difficult to accurately quantify the contribution of global warming to extreme events, there is no doubt about the increasing tendency of extreme events due to global warming and the severe impacts they may have on regional agriculture, ecosystems, and socio-economic systems ( Coumou and Rahmstorf, 2012; Perkins-Kirkpatrick and Lewis, 2020; WMO, 2012). Europe was affected by a severe heatwave in 2003, which caused more than 70,000 deaths (Robine et al., 2008) and irreparable damage to agricultural production

( García-Herrera et al., 2010; Bastos et al., 2020a; Bastos et al., 2020b).

However, in 2010, western Russia suffered from an even warmer summer, covering a record-breaking area of ~2 million km², causing approximately 55,000 heat-related deaths and a 30 % loss of crop yield (Barriopedro et al., 2011; McMichael and Lindgren, 2011; Russo et al., 2014; Shaposhnikov et al., 2014). Water stress caused by regional drought leads to increased mortality in high-latitude boreal forests (Peng et al., 2011) and decreased water use efficiency in Asian drylands (Lu et al., 2019; Tian et al., 2011), resulting in dramatic carbon emission, and similar findings also have been reported in low- and midlatitude forests (Mantgem et al., 2009; Phillips et al., 2009). It is not only "dry" events but also "wet" events that have caused serious

E-mail address: nanlv@rcees.ac.cn (N. Lu).

https://doi.org/10.1016/j.envint.2022.107509

<sup>\*</sup> Corresponding author.

impacts. For example, floods that occurred in Pakistan in 2010 covered one-fifth of the country's land area and affected approximately 20 million people (Hong et al., 2011).

These studies provide valuable results for our understanding of extreme events and their impacts. However, methods that focus on single extreme events are insufficient for defining and detecting all relevant conditions, which may lead to underestimation of the potential risks of extreme events (Leonard et al., 2013). The combination of multiple extreme events often makes the impact more severe or devastating than a single extreme event (Feng et al., 2019; Hao et al., 2021; Mazdiyasni and AghaKouchak, 2015; Mishra and Singh, 2010; Sharma and Mujumdar, 2017; Pan et al., 2020). Studies have shown that compound events significantly promote higher ozone concentration in the U. S. compared to the single extreme events of heatwave and atmospheric stagnation (by 10 %to 13 %), which can seriously affect air quality (Gao et al., 2020; Zhang et al., 2018). In 2010, heatwaves and droughts in Russia triggered wildfires and air pollution, with burned areas of more than one million hectares, resulting in a total economic loss of approximately 15 billion US dollars (Barriopedro et al., 2011; Grumm, 2011; Konovalov et al., 2011; Shaposhnikov et al., 2014; Witte et al., 2011). The crop yield loss caused by the simultaneous occurrence of dry and hot extreme events is much higher than that of either single event (Feng et al., 2019; Ribeiro et al., 2020).

To enhance the understanding of such complex multiple extreme events, two concepts have been established and are widely used. Compound climate extremes (com\_CEs, see Table S1 in the supplementary materials) refer to the occurrence of two or more extreme events in the same geographical area at the same time (Messori et al., 2021; Zscheischler et al., 2018). Cascading climate extremes (cas\_CEs) are defined as two or more extreme events (single CEs and/or com\_CEs) that occur consecutively or cumulatively without interruptions ( Pescaroli and Alexander, 2015; Sutanto et al., 2020). The urgency of research on com\_CEs and cas\_CEs is not only due to their greater impact but also because of their unpredictability. Although there is research on compound and cascading dry events at the pan-European scale (Sutanto et al., 2020) and global maps of the distribution of com\_CEs (Ridder et al., 2020), studies on the patterns of com\_CEs and cas\_CEs in drylands are lacking.

Drylands play an important role in dominating the trends and variability of the terrestrial carbon cycle (Ahlström et al., 2015; Piao et al., 2020; Poulter et al., 2014). However, they are also one of the most vulnerable regions on Earth (Fraser et al., 2011), and there is a risk of dryland expansion (Frierson and Scheff, 2015; Fu and Feng, 2014; Huang et al., 2015; Koutroulis, 2019; Lian et al., 2021; Schlaepfer et al., 2017; Yao et al., 2020), as well as vegetation death and land degradation due to water limitations (Berdugo et al., 2020; Liu et al., 2021a; Miao et al., 2015; Tao et al., 2015). When com\_CEs and cas\_CEs occur in fragile and rapidly changing drylands, their possible impacts become more disastrous and elusive. The broad area (37.9 % of the global drylands) and suitable locations (mostly located in the middle latitudes of the Northern Hemisphere) of Eurasian drylands make them the most diverse and frequent region for extreme events, which is suitable for our research (Maestre et al., 2021; Sivakumar, 2007) (Figure S1). In the past few decades, the rate of warming in Eurasian drylands has far exceeded the global average, especially in Central Asia and Mongolia, and the warming rate has reached 0.4 °C/decade in the past 40 years (Hu et al., 2014). In addition, some key drivers of extreme events in Eurasian drylands change rapidly (e.g., high-speed wind and extreme precipitation) (Sarhadi et al., 2018). All these signals indicate that more efforts need to be made to understand the patterns of com\_CEs and cas\_CEs in Eurasian drylands.

Therefore, the purpose of this study is to identify the types, spatial distribution hotspots, temporal rhythms, and centroid shifts of com\_CEs and cas\_CEs in the Eurasian drylands. It should be noted that although percentile-based threshold calculations for each grid cell can reduce the difference in these geographical regions, this method also has the

drawback of predicting the occurrence probability of each event in advance. To compensate for this deficiency of the percentile threshold method, we consider empirical values (details in the method). Based on reanalysis data (ERA5) released by the European Center for Medium-Range Weather Forecasts (ECMWF), we aimed to: 1) identify regional hotspots for the occurrence of com\_CEs and cas\_CEs; 2) determine the interannual and seasonal occurrence regimes of com\_CEs and cas\_CEs during 1979–2020; and 3) analyze the temporal and spatial migration of centroids of extreme events. Our results can provide initial guidance on which multivariate extreme events should be included in risk assessments in particular regions.

#### 2. Data and methods

#### 2.1. Data

Daily precipitation, temperature, and wind speed data covering Eurasian drylands are necessary for calculating the indices shown in Table 1. ECMWF reanalysis data version 5 (ERA5) was released by the ECMWF in 2019 (https://cds.climate.copernicus.eu/) (Hersbach et al., 2019). It provides global-scale climate variables with a time span from 1979 to 2020 and a significantly improved resolution over the previously released ERA-Interim (0.25°, ~31 km horizontal resolution of ERA5 compared with 79 km of ERA-Interim). ERA5 has the advantages of high resolution, wide coverage, and good fitting accuracy with observational data, which makes it widely used in the study of extreme climate events (Sutanto et al., 2020; Vitolo et al., 2019). We extract cooccurrence extreme events based on the ERA5 datasets and clipped by vector boundary of the Eurasian drylands, and finally obtain 406 rows \*804 columns \* 15341 days of result datasets covering Eurasian drylands.

### 2.2. Methods

## 2.2.1. Extracting compound and cascading climate extremes

The following three steps are used to complete the extraction of cooccurrence extreme events.

Step 1: Defining and extraction of single extreme events.

A set of indices (27 indicators) for the calculation and analysis of extreme events has been established based on daily temperature and precipitation and is widely used to assess global or regional extreme events (Alexander et al., 2006; Donat et al., 2013a; Donat et al., 2013b), providing a unified measurement standard for the study of climate extremes (Karl et al., 1999; Peterson, 2005; Peterson et al., 2001). The indices provide convenience for the comparison of extreme events in different regions. However, they also have some drawbacks. The threshold depends entirely on percentile-based indices, meaning that extreme events are bound to occur. If the 95th percentile is selected, the top 5 % of events in the historical time series are extreme events, which will overestimate or underestimate the occurrence of extreme events (overestimate: because of the setting threshold, 5 % of the extreme events will occur in the area without disaster; underestimation: areas with more than 5 % of disasters recorded only the top 5 % of events). It is a purely statistical method, and the accuracy relies strongly on historical data that needs to be verified by other indicators.

Therefore, we decided to extract extreme events by combining empirical values and percentile-based indicators, with duration considered when necessary (details are shown in Table 1). The large spatial span of the Eurasian drylands results in significant differences in temperature and precipitation; a high temperature of 38 °C would not cause a serious impact in India but would be fatal to northern regions such as Europe. Empirical values are determined mainly through three methods: (1) empirical values used in published literature (details in Table S2 in the supplementary materials), (2) definitions of extreme events in different nations, and (3) empirical values for extreme events recorded in the International Disaster Database (EM-DAT, https://www.

Table 1
Indicators of extract single extreme events.

Extreme events	Percentile-based thresholds		Empirical values	
Drought Heatwave	SPEI $<$ -1.0 $T_{\rm max}$ greater than 95th percentile of daily maximum temperature of 15-days window in the reference period and consecutive days more than 3 days	— Stefanon et al., 2012; Xu et al., 2016	one India: $T_{max} > 40^{\circ}C$ China: $T_{max} \ge 35^{\circ}C$ and consecutive days $\ge 3$ Eurone: $T_{max} > 30^{\circ}C$ and consecutive	— Huang et al., 2010; Hutter et al., 2007; Krzyżewska and Dyer, 2018; Ray et al., 2021; Sun et al., 2014
Low Temperature	$T_{\min}$ less than 95th percentile of daily manimum temperature of winter days in the reference period and consecutive days more than 3 days	I	days > 3  Threshold for the EM-DAT recording low temperature events (°C)	https://www.emdat.be/
Wind	d speed of windy	Martius et al., 2016; Telesca et al., 2020; Zhang et al., 2021		Yu and Zhong, 2019
High Precipitation	tile of daily precipitation of rainy days (≥1mm) in		None	1

Imax means daily maximum temperature (°C); T<sub>min</sub> means daily minimum temperature (°C); Wind<sub>max</sub> means daily maximum wind speed (m/s). Pre means daily precipitation (mm).

The reference period in this study refers to 1979–2020.

Empirical values of heatwave for more countries shows in Table S2 in Supplementary Materials.

emdat.be/). Areas lacking empirical values are replaced by empirical values for neighboring regions.

Combined with the indices and empirical values of each extreme weather and climate event (Table 1), the thresholds of each extreme event in each grid cell were calculated to determine whether they occur on the grid cell and generate a daily binary graph (0 represents no extreme event occurring on that day, and 1 represents extreme event occurrence) (Fig. 1 a). Extracting the data of the historical reference period for each grid cell to calculate the threshold value can effectively solve the applicability problem of a uniform threshold in different regions.

Step 2: Defining and extracting com\_CEs.

Single day or consecutive days which satisfies the indicators (for a specific climate extreme) list in Table 1 counts as one single climate extreme event. By overlapping the binary graph of five single extreme events that have been assigned unique values daily (Fig. 1 b and c), it is possible to determine the occurrence of com\_CEs on a given day and location (longitude, latitude). The traditional binary graph divides the attribute value of each grid cell into zero (no extreme event occurred) and one (extreme event occurred). It is easy to determine the number of events that occur after stacking according to the value. However, the composition of specific extreme event types is unclear. Therefore, we improved the algorithm by assigning different values to five single extreme events to ensure uniqueness of the results after stacking. The unique values of each extreme event are shown in Table 2, while the results after stacking are shown in Table S3 in the supplementary materials.

Step 3: Defining and extracting cas\_CEs.

Cas CEs refer to two or more extreme events (single CEs and/or com\_CEs) that occur consecutively or cumulatively without interruptions. Therefore, we must determine the start and end times (t<sub>1</sub>, t<sub>2</sub>) of each cas\_CE by overlapping the day-by-day binary graphs of single extreme events. The types of single extreme events that occur during t<sub>1</sub>-t<sub>2</sub> are then understood, and the grid cell values in this period are assigned to determine the distribution of cascading events after stacking (the unique values of single extreme events are shown in Table 2; see Table S2 in the supplementary materials for the results after stacking). It should be emphasized that for cas\_CEs, we pay more attention to temporal continuity (that is, a period which is not interrupted by no hazard day). Thus, we first determine the start and end times (t1, t2) of each cas CEs and then explore the specific types of extreme events occurring during the period of t<sub>1</sub>-t<sub>2</sub> and classify them. We do not place strict restrictions on the time sequence of extreme events that constitute cas -CEs, there will be more combinations (far more than the 26 listed in Table S2) if we consider the time sequence of extreme events in  $t_1-t_2$ . Similarly, we do not require extreme events in each day to be a single extreme event, and it is also considered feasible to embed the same combination of com\_CEs. As shown in Fig. 1 d, cas\_DH is detected during t<sub>1</sub>-t<sub>2</sub> for a total of 4 days, with com\_DH occurring on day 3 and day 4.

## $2.2.2. \ \ Calculation \ of \ return \ period \ for \ hotspots \ detection$

The return period (RP) means the average time interval between recurrences. A smaller RP indicates that more extreme events occurred in this region during the same time period. Hotpots for extreme events are defined as regions with a high frequency of extreme events, which also means regions with smaller RP values. We calculate the joint occurrence probability of extreme events for each grid cell, that is, the ratio of the number of days in which extreme events occur for a grid cell to the total number of days during the study period. The RP is the result of the inverse of occurrence probability divided by the number of days during the study period.

Taking com\_DH (see Table S1) as an example, i represents the specific date during 1979–2020 ( $1 \le i \le 15341$ ),  $D_i$  indicates whether drought occurred on this day, and  $H_i$  does the same but for heatwaves. com\_DH $_i$  refers to the occurrence of compound drought and heatwave events. The RP of com\_DH is calculated using formulas (1)–(3).

# (a) Extract time series of a location and generate a day-by-day binary graph of a single extreme event

Compound events

2.11000 2.10001

2.00110

3.10011

DWP

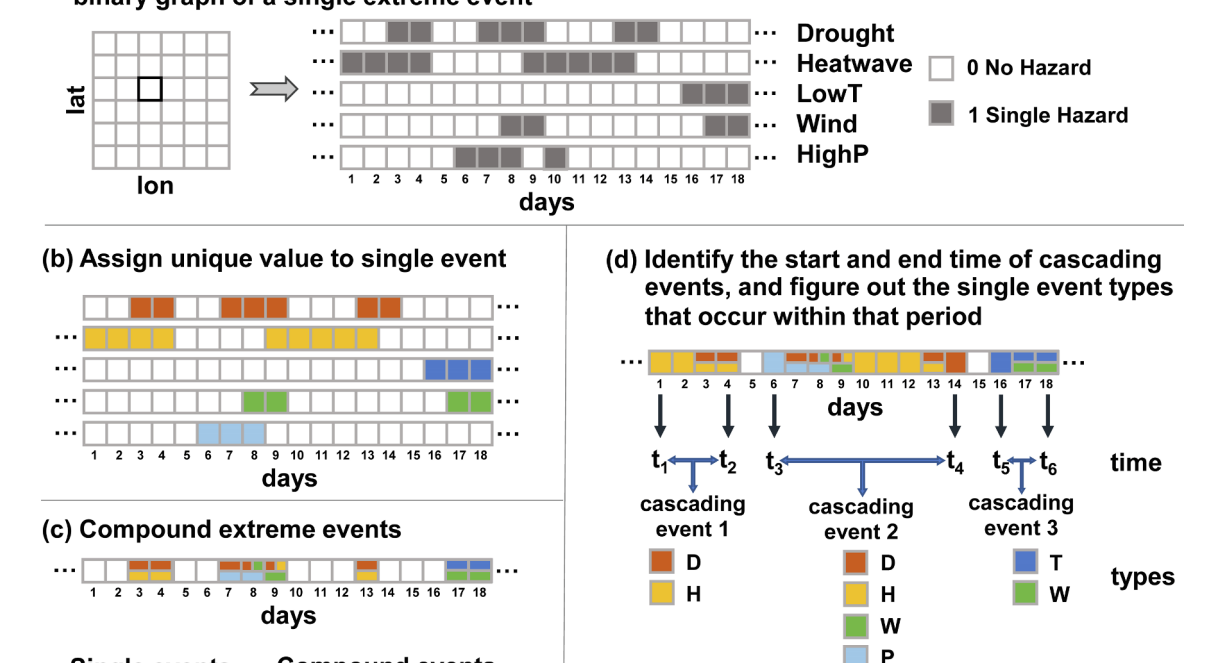


Fig. 1. Schematic diagram of compound/cascading extreme events calculation method Note: Fig. 1 is only used to understand the extraction method of extreme events and does not represent the actual occurrence.

 Table 2

 Unique values and abbreviation of five single extreme events.

Single events

1.1

1.01

1.001

1.0001 W

1.00001 P

Value	Extreme events	Abbreviation	Explanation
0	None	_	No extreme event
1.1	Drought	D	Single extreme event
1.01	Heatwave	H	Single extreme event
1.001	Low Temperature	T	Single extreme event
1.0001	Wind	W	Single extreme event
1.00001	High Precipitation	P	Single extreme event

$$com_{-}DH_{i} \begin{cases} = 1whenD_{i} = 1andH_{i} = 1\\ = 0others \end{cases}$$
 (1)

$$P(com\_DH) = \frac{\sum_{1}^{alldays} com\_DH_i}{alldays}$$
 (2)

$$RP(com\_DH) = \frac{1}{P(com\_DH) \times 365}$$
(3)

## 2.2.3. High-frequency events selected for time series analysis in different subregions

Eurasian drylands are divided into eight climate subregions based on the adjustment of the partitions proposed by the IPCC (IPCC, 2012) (details are shown in Figure S2 in Supplementary Materials), and the most frequent com\_CEs and cas\_CEs in each subregion are extracted for further time series analysis. Specifically, we calculate the number of days per unit area of extreme events occurring in each subregion to determine the rank of occurrence of extreme events (results are shown in Section 3.2.1). The number of days per unit area rather than the total

number of days in each subregion is chosen to reduce the impact of the subregion area on the results.

## 2.2.4. Analyzing the centroids migration of the extreme events

📕 2.11000 DH 🔡 4.11011 DHWP 📕 2.00110 TW

5 6 7 8 9 10 11 12 13 14

Cascading events

A new density-based clustering algorithm, ST-DBSCAN (Spatial and Temporal-Density-Based Spatial Clustering of Applications with Noise) (Birant and Kut, 2007), is widely used in the analysis of hotspot clusters of extreme events or disasters because of its outstanding performance in clustering spatial-temporal data (Cai et al., 2020; Di Martino et al., 2018; Liu et al., 2021b; Sitanggang et al., 2020; Wang et al., 2020b). To determine whether a set of points is sufficiently similar to be considered a cluster, ST-DBSCAN accepts two radiuses value (eps1 and eps2) to define the range of data within temporal neighbors and their corresponding spatial values. In clustering, two radiuses (eps1 and eps2) are considered instead of one, which is also the biggest difference between ST-DBSCAN and DBSCAN methods. This makes clustering expand from two-dimensional plane to three-dimensional space. The two radius variables selected in our study are space distance and time span (days) respectively. When a point in the neighborhood of a given radiuses has to contain at least a minimum number (MinPts) of other points, it becomes a cluster, and the point is defined as the core object. The ST-DBSCAN algorithm can identify clusters of any shape without the need to set the number of clusters in advance. However, when there is density tilt in the clustering process, it is likely to be easy to find the problem of the cluster being too long or the clustering not working well. We refer to the barycenter transfer method proposed by Liu et al. (2018) to improve the ST-DBSCAN clustering algorithm and applied it to this study. Based on the algorithm program provided by Birant et al. (2017) and combined with the improved solutions of three types of gravity center shifting proposed by Liu et al. (2018), we convert the formulas they provided

into code in R programming software to form a complete algorithm program. The version of R programming software is R x64 4.0.3, which can be downloaded in <a href="https://www.r-project.org/">https://www.r-project.org/</a>.

## 3. Results

## 3.1. The hotspots of compound and cascading extreme events

Compound drought and heatwave events (com\_DH) occurred broadly in the Eurasian dryland during 1979-2020, except for in the Qinghai-Tibet Plateau and high-latitude regions, with the highest frequency in the Arabian Peninsula and the southeastern part of the Eastern European Plain (return period of approximately 1-2 years), and other regions such as India, the Iranian Plateau, and the Mongolian Plateau were sub-high frequency occurrence areas, with a return period of approximately 3 years (Fig. 2 a). The occurrence of com DT was located at high latitudes, especially in eastern Siberia, with a return period of 2–3 years, and even the return period in some areas (such as the coast of the Arctic Ocean) was less than one year (Fig. 2 b). Some events displayed remarkable regional signatures; the hotspots of com DW were concentrated in Central Asia, the Qinghai-Tibet Plateau, and the Mongolian Plateau, where a once-a-year com DW event often occurred (Fig. 2 c). Other compound events related to wind had similar regional hotspots, but the difference was that com\_WP in Central Asia had a much shorter return period than com\_DW (half a year compared with 1-2 years), and the coastal area of the Arctic Ocean was also diagnosed as a high-incidence area of com\_WP (the return period of the hotspot area was usually half a year), which was not a hotspot of com\_DW (Fig. 2 i and Figure S3 in supplementary materials). The com\_DP had little clear regionality over the Eurasian drylands, and the return period was more than 21 years (Fig. 2 d). Multiple com\_CEs (≥3 events compounded),

with a return period of over 21 years, are not discussed in detail here (Figure S4 in the supplementary materials).

com\_CEs emphasize simultaneous occurrence in time, while cas\_CEs emphasize that they occur successively in time, and complex events that are composed of the same single extreme events often lead to similar regional hotspots. The hotspot area of cas\_CEs was significantly smaller than that of com\_CEs, and the return period of cas\_CEs was significantly shorter than that of com\_CEs (Figs. 2 and 3). However, there were some exceptions: the hotspots of cas\_WP were consistent with those of com\_WP, but the return period was longer than that of the compounded event, which meant that com\_WP occurred more frequently in these areas (Fig. 2 i and Fig. 3 i). Hotspots for cas\_DP were found in Central Asia and were scattered in other regions (Fig. 3 d).

In general, the majority of com\_CEs and cas\_CEs were composed of two single extreme events, and the occurrence of more than two extreme events was uncommon. The combination of DH, DT, DW, and WP should attract our attention because they have prominent spatial hotspots and a short return period. com\_CEs and cas\_CEs often had similar geographical hotspots, and the occurrence of cas\_CEs was even higher, which has not been reported in previous studies. The Eastern European Plain, Mongolian Plateau, and Central and West Asia were the hotspots for the majority of multivariate extreme events.

## 3.2. Seasonality and interannual variations of compound and cascading extreme events

## 3.2.1. Relative importance of extreme events in different geographical regions.

Although there are 26 types of extreme event combinations in theory (Table S2 in supplementary materials), the results show that the extreme events in each subregion were mainly dominated by several types of

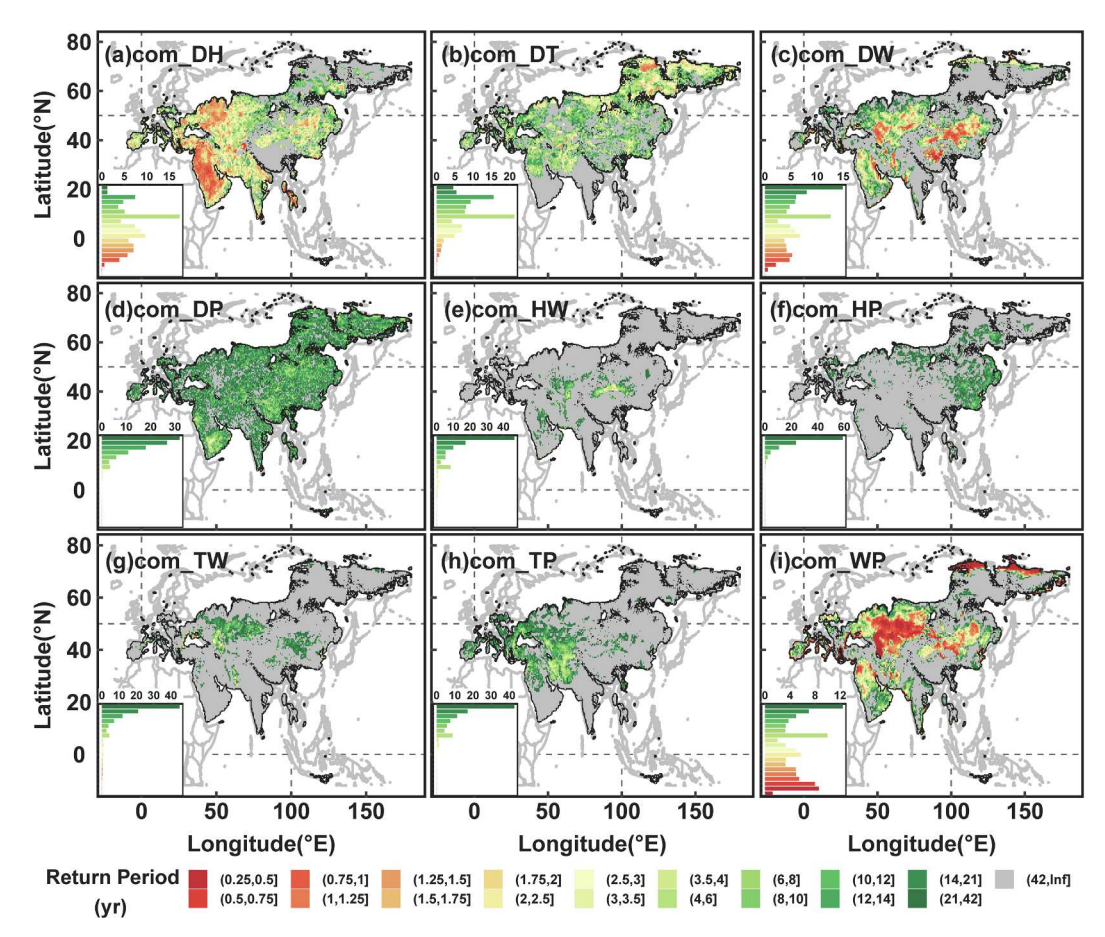


Fig. 2. Return periods for com CEs in Eurasian drylands (two events compounded).

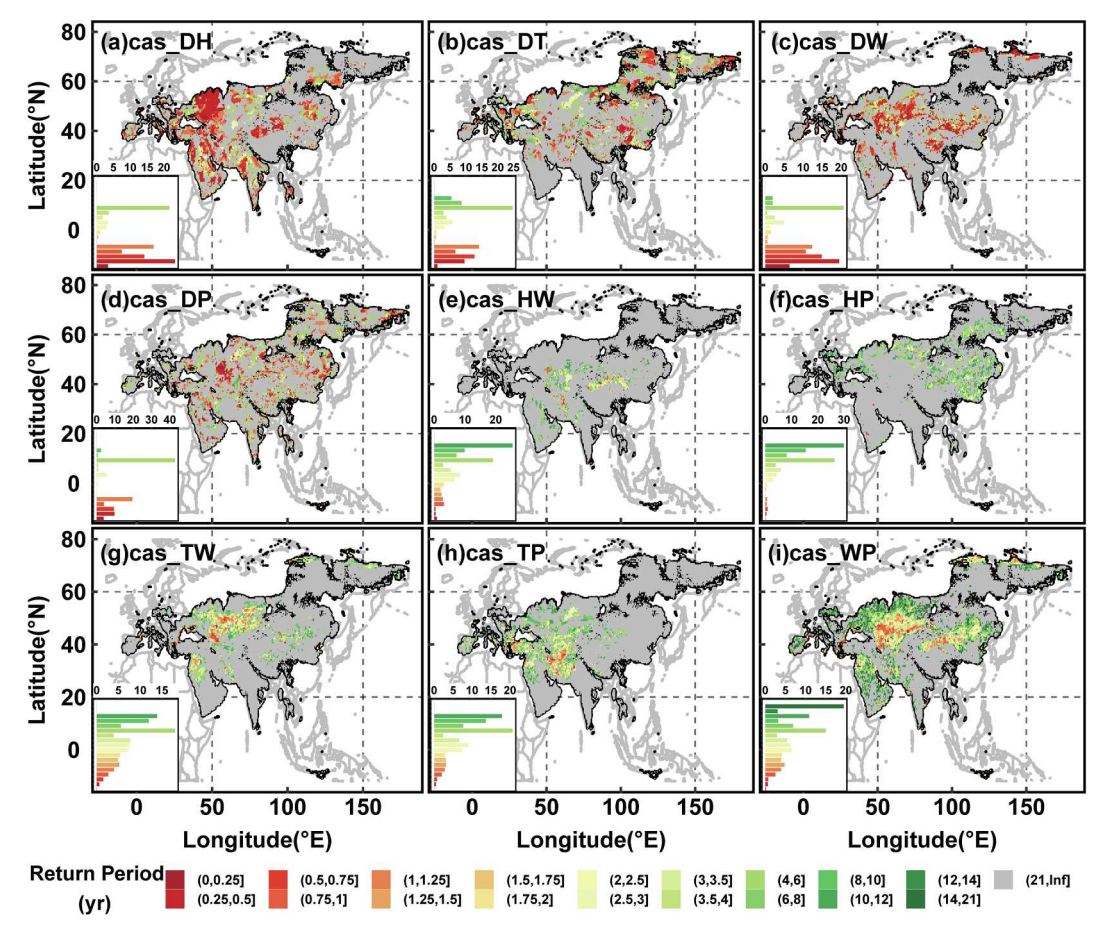


Fig. 3. Return periods for cas\_CEs in Eurasian drylands (two events cascaded).

events. The five most typical com\_CEs accounted for more than 90 % (93–99 %) of all com\_CEs (Fig. 4), and the proportion of cas\_CEs ranged from 79 % to 93 % (Fig. 5).

Specifically, the typical types of com\_CEs in the seven subregions are completely consistent except for CNEU, including com\_DH, com\_DT, com\_DW, com\_DP, and com\_WP. Neighboring subregions tended to have similar compositions and occurrences of extreme events, whereas in the CNEU, MED, and WAS subregions located in the western part of the midlatitudes, com\_DH played a dominant role (Fig. 4a, b, d). In the eastern part of the mid-latitude region, com\_DW gradually emerged, and the frequency of com\_DW equalized or even surpassed that of com\_DH (Fig. 4 e, f, g). In contrast to the mid-latitudes, com\_DH dominated com\_CEs in the low-latitude region, and the occurrence of other events was rare (Fig. 4 h). Com\_DT, which occurred less frequently in other regions, with an occurrence of nearly 10 days for each grid cell in the NAS, became the dominant event type at high latitudes (Fig. 4 c).

The typical types of cas\_CEs were similar to those of com\_CEs, but the dominance of cas\_DH and cas\_DW was weakened. The occurrence frequency of cas\_DP was significantly higher than that of com\_DP, especially in mid-latitude areas where the frequency of cas\_DP changed from to 2–3 to 10–15 days. The importance of cas\_DP gradually became prominent (Fig. 5 b, d, e, f, g).

## 3.2.2. Seasonal differentiation of extreme events

The most representative types of com\_CEs and cas\_CEs are identified in Figs. 4 and 5, and their seasonal differentiation should be analyzed (the results are shown in Figs. 6 and 7). The western subregions of the Eurasian drylands and SAS were dominated by com\_DH in the summer days (summer is from June to August for most Northern Hemisphere areas, but April to June for SAS), while in other seasons, multiple

com\_CEs co-existed. com\_DH accounted for 90 % or more of the extreme events in summer (Fig. 6 a, d, f, g), but the proportion was approximately 50 % in the eastern subregions (Fig. 6 b, c, h). The com\_DW was prevalent in the EAS and TIB regions in spring and autumn (Fig. 6 e, h), while in the western subregions at mid-latitudes, it was dominated by com\_DW in spring but com\_WP in autumn (Fig. 6 a, d, h). com\_DT was the dominant type of com\_CEs in winter in the EAS and NAS due to temperature constraints (Fig. 6 c, h), accounting for more than 85 % of extreme events in winter in these two regions.

The distribution of cas\_CEs was more complex, with less dominance of one cas\_CEs. Specifically, unlike com\_CEs, cas\_DH was no longer the dominant type during summer in all Eurasian drylands but was still dominant only in CNEU, WAS, MED, and SAS (Fig. 7 a, d, f, g). The cas\_DW was a high-frequency event in the Tibetan Plateau in spring (Fig. 7 e), and cas\_DT was still the main type in winter in the NAS and EAS (Fig. 7 c, h). cas\_DP occurred frequently from August to November in SAS, EAS, and NAS (Fig. 7 c, g, h), which might be related to water vapor transport from the ocean.

In terms of the seasonality of extreme events (Figs. 6 and 7), temperature-constrained com\_DH and cas\_DH prevailed in summer and dominated in low- and mid-latitude areas, while the peak season of temperature-limited com\_DT and cas\_DT occurred in boreal winter. Compared to summer and winter, the composition of extreme events in spring and autumn was more diverse. com\_DW prevailed in the spring and autumn in the eastern region of Eurasian drylands, whereas com\_DW prevailed in spring, and com\_WP mainly occurred in the autumn in the western region of Eurasian drylands. The cas\_CEs in spring and autumn were not similar to com\_CEs, which were dominated by only one com\_CEs, but multiple cas\_CEs co-occurred frequently.

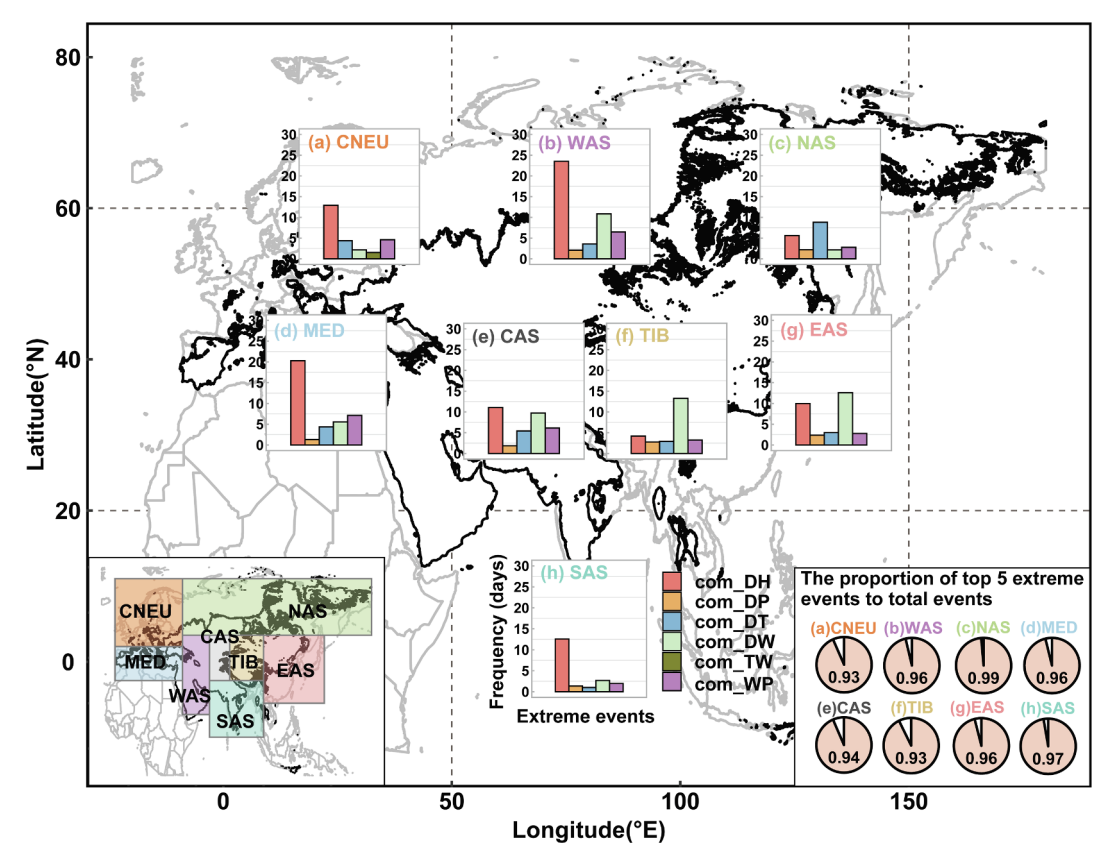
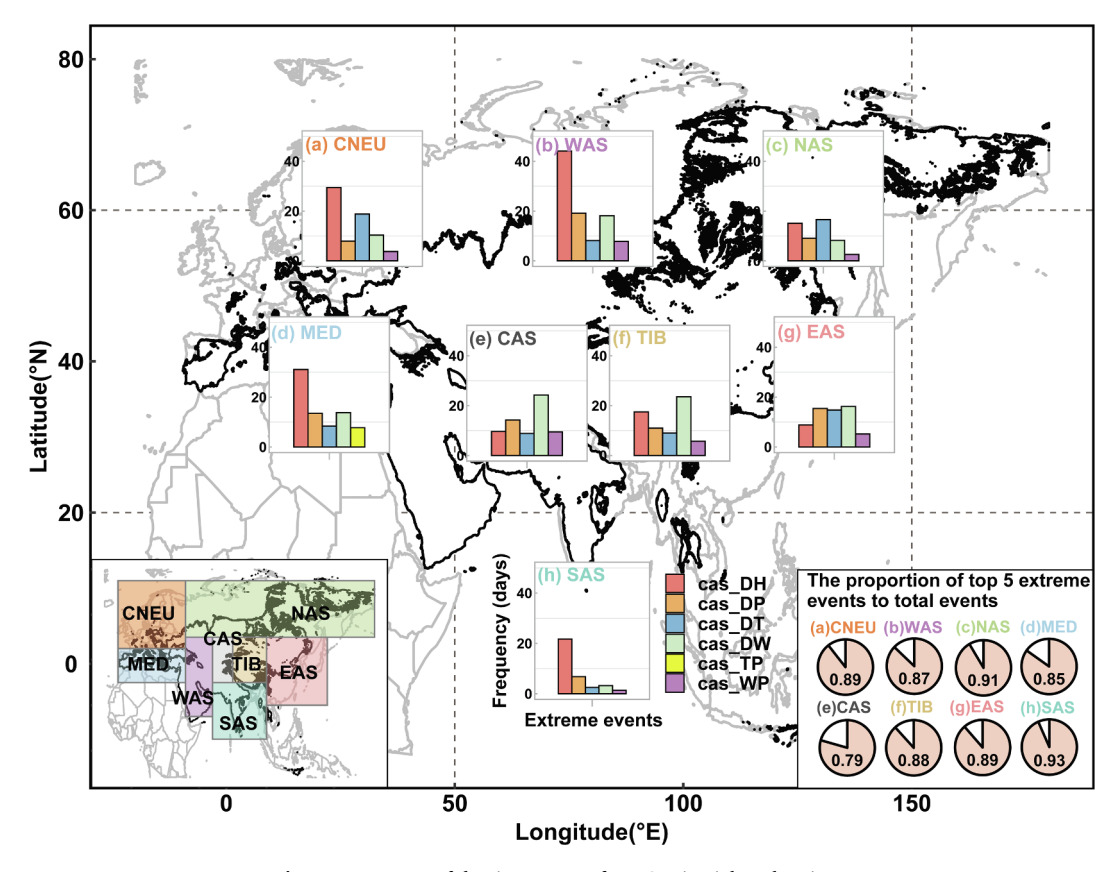
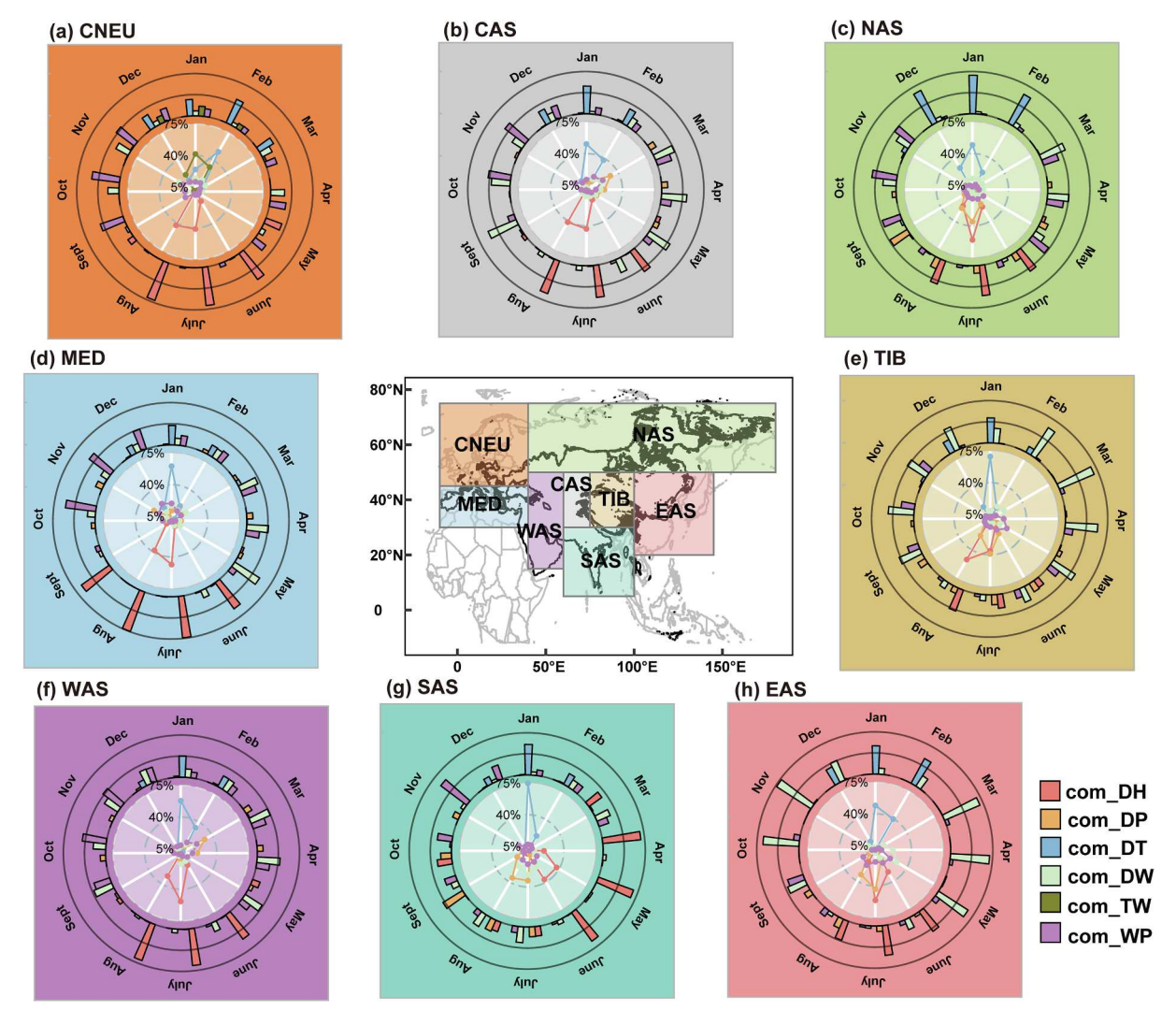


Fig. 4. Frequency of dominant type of com\_CEs in eight subregions (Y-axis indicates the average number of days per grid recorded, i.e., the ratio of the total number of days of an extreme event occurring in this subregion to the total area of this subregion.).



 $\textbf{Fig. 5.} \ \ \textbf{Frequency of dominant type of } \textbf{cas\_CEs in eight subregions}.$ 



**Fig. 6.** Seasonal distribution of typical com\_CEs in each subregion. (The radar diagram inside the **Figure** represents the seasonal distribution of the top 5 typical com\_CEs in each subregion, that is, the ratio of the number of days of an extreme event in each month to the total number of days of the event in the whole year. The gray dotted circle represents 40%, and the maximum value is 75%. The polar coordinate histogram of the outer circle represents the dominant extreme events in each month in a certain subregion, that is, for a certain month in a certain subregion, the proportion of the number of days of an extreme event in the total number of days of all extreme events in that month. The three solid black circles represent 0, 0.5, and 1, respectively.).

## 3.2.3. Interannual variability of extreme events

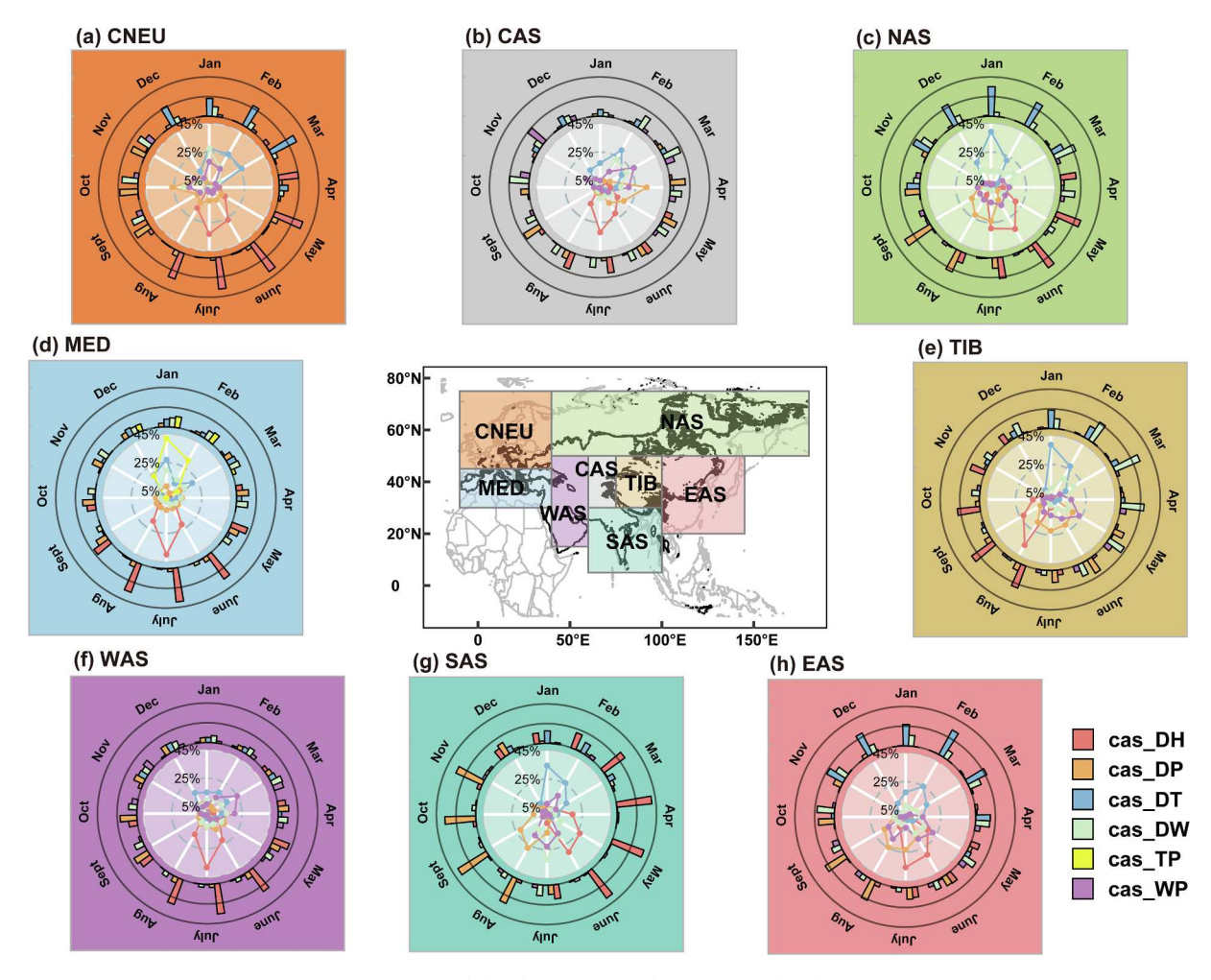
The inter-annual distribution of com\_DH had obvious regularity, and the average annual occurrence days in CNEU, MED, CAS, and WAS showed a significant turning point around 2000, increasing from the previous 0.2 days to 1–2 days (Fig. 8 a, b, d, f). The occurrence days in EAS, NAS, and TIB were stable before 2000 and then increased and reached a peak value in 2010, followed by a decrease (Fig. 8 c, e, h). In SAS, there was an increasing trend, followed by a decrease and then an increase, with two turning points in 1990 and 2000, respectively. Another compound extreme event with significant interannual variability was com\_DW, whose annual occurrence days in EAS began to increase after 2000 (Fig. 8 h), while the number of occurrence days in the CAS and TIB subregions gradually increased after 2000, and the trend changed from increasing to decreasing in 2010 (Fig. 8 b, e).

The annual occurrence of cas\_CEs was generally longer than that of com\_CEs. The interannual variation in cas\_DH was similar to that of com\_DH, showing an increasing trend in the MED, CAS, and WAS subregions, with a turning point in 2000 (Fig. 9b, d, f), whereas in the EAS, NAS, TIB, and CNEU subregions, it first increased and then decreased. The increasing trend started around 2000 and peaked around 2010 (Fig. 9 a, c, e, h). The cas\_DH in South Asia showed a trend of first

increasing, then decreasing, and then increasing, with two turning points in 1995 and 2005 (Fig. 9 g). However, unlike com\_CEs, cas\_DP events have significantly changed in recent years. The cas\_DP events in the EAS, NAS, CAS, and WAS subregions began to show an increasing trend around 2000, peaked around 2010, and then decreased (Fig. 9 b, c, f, h). The cas\_DP in CNEU has shown a sharp increasing trend since 2010 (Fig. 9 a).

## 3.3. The shift of the centroid of extreme events

According to the density clustering method ST\_DBSCAN, the location and occurrence time of the most representative typical extreme events are extracted. Five representative com\_CEs contain data points ranging from 70,000 to 260,000, and six typical cas\_CEs contain data points ranging from 120,000 to 290,000. In the specific calculation process, the two radius variables selected in our study are space distance (eps1, grid cell distance) and time span (eps2, days) respectively. When eps1 and eps2 are both set to 8, the maximum number of data points within the cluster radius exceeds 1000, which is a little large for our analysis data. Therefore, we calculated the maximum number of points within the cluster radius under different combinations of eps1 and eps2 ranging



 $\textbf{Fig. 7.} \ \ \textbf{Seasonal distribution of typical } \ \textbf{cas\_CEs in each subregion.}$ 

from 1 to 7, respectively. The MinPts is taken as 50 %, 45 % and 40 % of the number of points within the cluster radius under different combinations. We use different combinations of eps1, eps2 and MinPts for clustering, and finally determine the optimal parameter combinations of com\_CEs as 6,2,153 and cas\_CEs as 4,4,188. Based on clustering results, spatial shift of the centroid over time is analyzed (Figs. 10 and 11).

From the analysis results of the centroid of the com CEs, it can be seen that the typical com DH events occurred sporadically before 2000 and were mainly concentrated in the Indian Peninsula and the central and northern parts of Central Asia. The frequency of occurrence increased significantly in the past two decades (especially from 2009 to 2019), and it was broadly distributed in the middle and low latitudes of the Eurasian drylands, with two hotspots in West Asia (35.8 %) and northern East Asia (14.2 %) (Fig. 10 a). The distribution of the centroid of com DP was similar to that of com DH, and the number of centroids increased sharply from 2000, with two concentrated areas located in North Asia and West Asia (28.43 % and 22.55 %, respectively) (Fig. 10 b). In contrast to the obvious time aggregation of com\_DH and com\_DP, the frequency of com\_DT, com\_DW, and com\_WP fluctuated over the past four decades (as shown in the histogram in Fig. 10). It was worth noting that the main occurrence area of com\_DT events in the past 42 years was North Asia (63.27 %), but the hotspots showed obvious characteristics of shifting from high latitude to low latitude areas over time (Fig. 10 c). The com\_WP events clustered at the boundary of West Asia, North Asia, and Central Asia, and the hotspot did not change over time (WAS 39.5 %, NAS 26.89 %, CAS 25.21 %) (Fig. 10 e). There was no

centroid shift in com\_DW, which might have occurred in the midlatitude regions (Fig. 10 d).

The occurrence of typical cas\_CEs was much less than that of com\_-CEs, and there was a less obvious centroid shift in the regional distribution. In the past 40 years, the centroid of cas DP was scattered throughout Eurasian drylands and occurred more frequently in South Asia and Central Asia in the early stage, shifting to North Asia and West Asia in recent years (NAS 36.59 %, WAS 17.07 %) (Fig. 11 b). In the historical stage, cas\_DW events were mainly distributed in the Central and West Asia region and high-latitude areas such as the coast of the Arctic Ocean, but in recent years, they have mostly occurred in the Central and West Asia region and northern China (Fig. 11 d). Except for the two cas CEs above, the centroids of the other cas CEs did not experience a shift. Nearly 40 % of the centroid of the cas DH events occurred in West Asia (39.34 %), especially in the Arabian Peninsula (Fig. 11 a), which was also a hotspot of the com\_DH events. This may be due to the fact that the subtropical high pressure prevails in this area all year round and causes less precipitation. In addition, the underlying surface here is desert, which has the characteristics of rapid heating, resulting in frequent extreme drought and heatwave events. The cas\_DT event was mostly distributed at high latitudes (NAS accounted for 66.67 %), particularly in the Mongolian Plateau (Fig. 11 c). The cas\_WP events were concentrated in the boundary regions of West Asia, North Asia, Central Asia, and the Inner Mongolia region of China at 40°N over the past four decades (Fig. 11 f). The centroid of the cas\_TP events has always been in Central and West Asia (Fig. 11 e).

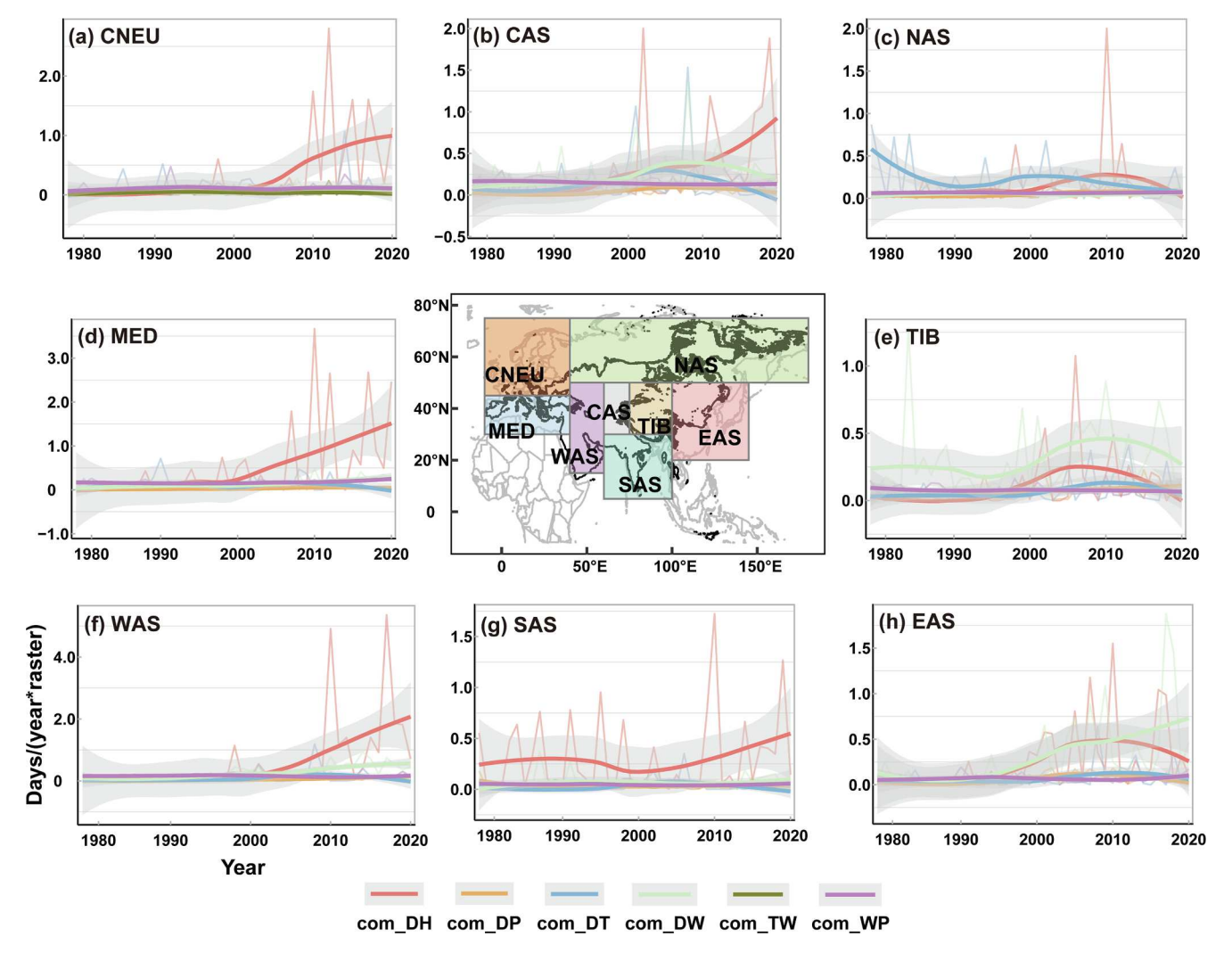


Fig. 8. Interannual variation of average occurrence days for each grid cell of major com\_CEs in each subregion.

#### 4. Discussion

## 4.1. Hotspots and drivers behind the occurrences of CEs

We identify hotspots of com\_CEs and cas\_CEs in Eurasian drylands. The hotspots of dry-hot extreme events show a high degree of similarity in the overall patterns of dry-hot CEs when compared with global and regional results (Diffenbaugh et al., 2007; Hao et al., 2018; Ridder et al., 2020; Sharma and Mujumdar, 2017; Vogel et al., 2021). The occurrence of summer dry-hot extreme events in the Northern Hemisphere midlatitudes is associated with anomalous jet stream circulation patterns characterized by persistent high-amplitude quasi-stationary Rossby waves (Eastern Europe and EAS controlled by wave 5, while Western Europe and WAS were controlled by wave 7) (Coumou et al., 2014; Kornhuber et al., 2016; Screen and Simmonds, 2014). The anomalous circulation regimes lead to persistent surface weather conditions, which greatly increase the probability of occurrence of extreme heat events in the mid-latitudes, as confirmed in 2003, 2010, and 2018 extreme heatwave events (Barriopedro et al., 2011; Kornhuber et al., 2019a; Kornhuber et al., 2019b; Liu et al., 2020). At the regional scale, the cooccurrence of dry-hot conditions can be attributed to stationary anticyclones that block westerly flow in the midlatitudes, thereby inducing precipitation and temperature anomalies in and around the blocked area (Röthlisberger and Martius, 2019). Sudden and intense heat can lead to abrupt increases in air temperatures, further strengthening local land--atmosphere feedbacks via soil desiccation, and dry soils in these

regions also contribute to the escalation of air temperatures (Hauser et al., 2016; Schumacher et al., 2019).

The occurrence of wind and high precipitation was often concentrated in western mid-latitude regions such as MED and CNEU during autumn, which has also been confirmed by regional research results (Raveh-Rubin and Wernli, 2015). Large-scale wind and precipitation extremes in the mid-latitudes often occur simultaneously near extratropical cyclones such that the affects regions often overlap, which has also been verified in some studies (Martius et al., 2016; Raveh-Rubin and Wernli, 2015). On the other hand, based on historical observational data (1971–2000), the seasonal variability of precipitation in the Eurasian dryland is large, especially in West Asia, Central Asia, and the Mongolian Plateau, which will lead to an abnormal increase in precipitation during the rainy season, thereby increasing the occurrence of wet extreme events such as heavy precipitation (Konapala et al., 2020; Pascale et al., 2014; Pascale et al., 2015).

## 4.2. Datasets need to be provided so that more empirical value can be involved in the analysis of extreme events

Our results are supported by the global and regional assessments of com\_CEs and cas\_CEs, but there are still some differences; the results of global com\_CEs show that com\_DH is prevalent in the mid-latitudes, including the Qinghai-Tibet Plateau region (Ridder et al., 2020), but it is not a hotspot of com\_DH in our results. This is mainly because an empirical value is considered in our calculation process. The

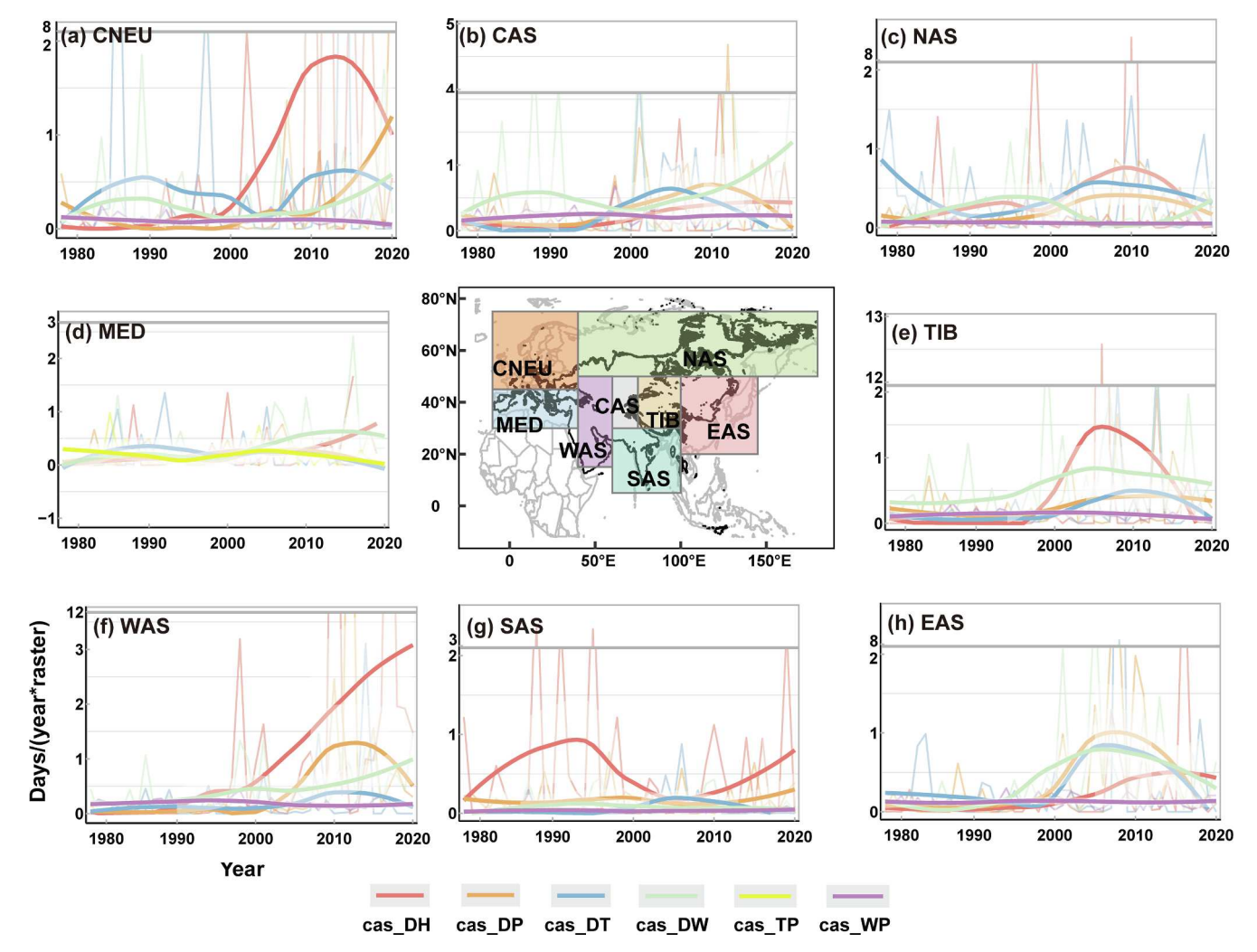


Fig. 9. Interannual variation of average occurrence days for each grid of major cas CEs in each subregion.

temperature of the Qinghai-Tibet Plateau has increased abnormally in recent years owing to global warming. If we rely solely on the percentile-based threshold, we will identify these abnormally high temperature values as extreme events, and the setting of the empirical values will avoid misjudgment.

The empirical values obtained from other sources are very limited. Although we have taken the empirical values from published literature, national standards, and EM-DAT into consideration, we still could not achieve good performance in terms of spatial coverage. The EM-DAT database has recorded more than 20,000 events since 1900, but only if the events are of great size and impact, and records of events that do not meet the requirements are discarded. However, we also know that extreme events that are not compiled into EM-DAT are less severe but occur more frequently, and that the effects of cascading and compound extreme events made up of these extreme events can be even greater than our estimate. Therefore, a shared global database of extreme event records is necessary, which can help us better understand co-occurring events.

## 4.3. Mid-latitude regions may suffer extreme events that have never occurred before

Our analysis of the spatial shift of the centroid during 1979–2020 indicates that the frequency of com\_DH increase significantly after 2000 and form clusters in the Mediterranean, WAS, and northern EAS, which is also found in Hao's research (2018). It has been confirmed that the

increase in the number of dry and hot compound events is primarily driven by temperature changes rather than a lack of precipitation (Diffenbaugh et al., 2007; Vogel et al., 2021). Coincidentally, summertime compound hot extremes in the northern hemisphere have become more frequent and intense in the past five decades, especially in the Mediterranean and Mongolia (the frequency increase with a speed of 1.5 days/decade in those areas compare with an average increase of 1.03 days/decade, and an intensity increase of 0.5 °C/decade compare with the regional average of 0.28 °C/decade) (Wang et al., 2020a). Studies on summer warming in Eurasia also found that the most predominant amplified warming occurred over Europe, West Asia, and Northeast Asia (Hong et al., 2017).

The increase in temperature directly leads to the occurrence of heatwaves, and the regional land–atmosphere feedback further enhances the extreme temperature changes. Temperature is not only a driver of heatwave events; long-term persistent high temperatures can lead to increased terrestrial radiation which further intensifies near-surface heat, accelerating the increase in surface evaporation, which increases the probability of extreme drought-related events. We believe that the Mediterranean, WAS, and Northern EAS will face greater threats from com\_DH in the future.

Unlike DH, which mostly occurs in middle and low latitudes, hotspots for DT are mainly distributed at high latitudes owing to temperature constraints. However, the centroid of the DT showed migration from high latitude to middle latitude areas during 1979–2020. Some studies have also found that the frequency of extreme low temperature

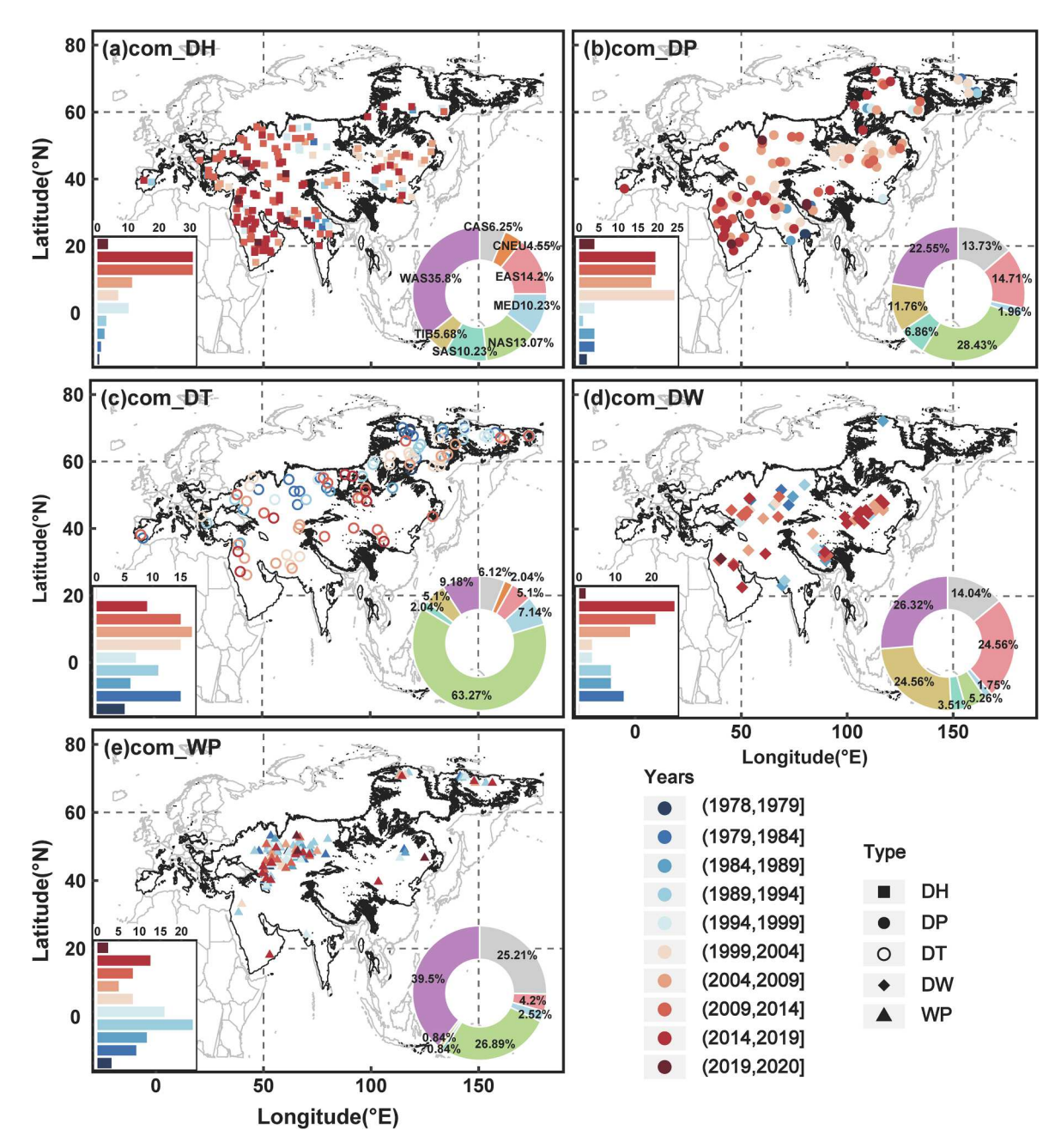


Fig. 10. Temporal and spatial shifting in centroid of typical com\_CEs. The histogram in the lower left corner represents the frequency of com\_CEs in different time periods (%); the ring graph in the lower right corner indicates the occurrence frequency of com\_CEs in eight subregions (%).

events in the northern hemisphere is declining in the early stage, but it has increase significantly in the past ten years. It is worth noting that the hotspots are no longer high latitudes north of 50°N but are mainly concentrate in the mid-latitudes of the Northern Hemisphere (Cohen et al., 2014; Johnson et al., 2018), which is consistent with our observations.

The migration of hotspots of DT may be related to the warm Arctic-cold continent (WACC) (Chen et al., 2018; Overland et al., 2011) or, more specifically, warm Arctic-cold Eurasian (WACE) (Mori et al., 2014). WACE is characterized by accelerated warming in the Arctic, cooling in the mid-latitudes of Eurasia, and accelerate Arctic ice loss. The cold anomaly spreads zonally from Southern Europe to East Asia (Mori et al., 2019; Petoukhov and Semenov, 2010; Tang et al., 2013). Furthermore, the negative phase of the North Atlantic Oscillation (NAO) and planetary waves are also considered to cause lower temperatures in the mid-latitudes of the Northern Hemisphere (Cohen et al., 2014;

Francis and Vavrus, 2015; Overland et al., 2011; Tang et al., 2013; Ye and Messori, 2020).

These findings suggest that the mid-latitudes of the Eurasian dryland, particularly around Mediterranean, Central, and West Asia and the Mongolian plateau, are emerging as new hotspots for events that have never occurred before. This has also been detected by changes in planetary waves, which show that mid-latitude regions will face more extreme events in the future (Kornhuber et al., 2019a; Wang et al., 2013).

#### 5. Conclusion

We have identified the representative com\_CEs and cas\_CEs and their hotspots in Eurasian drylands and analyze the seasonality, interannual variability, and spatial shift of the centroid of these extreme events. Our results show that the representative types and hotspots of com\_CEs and

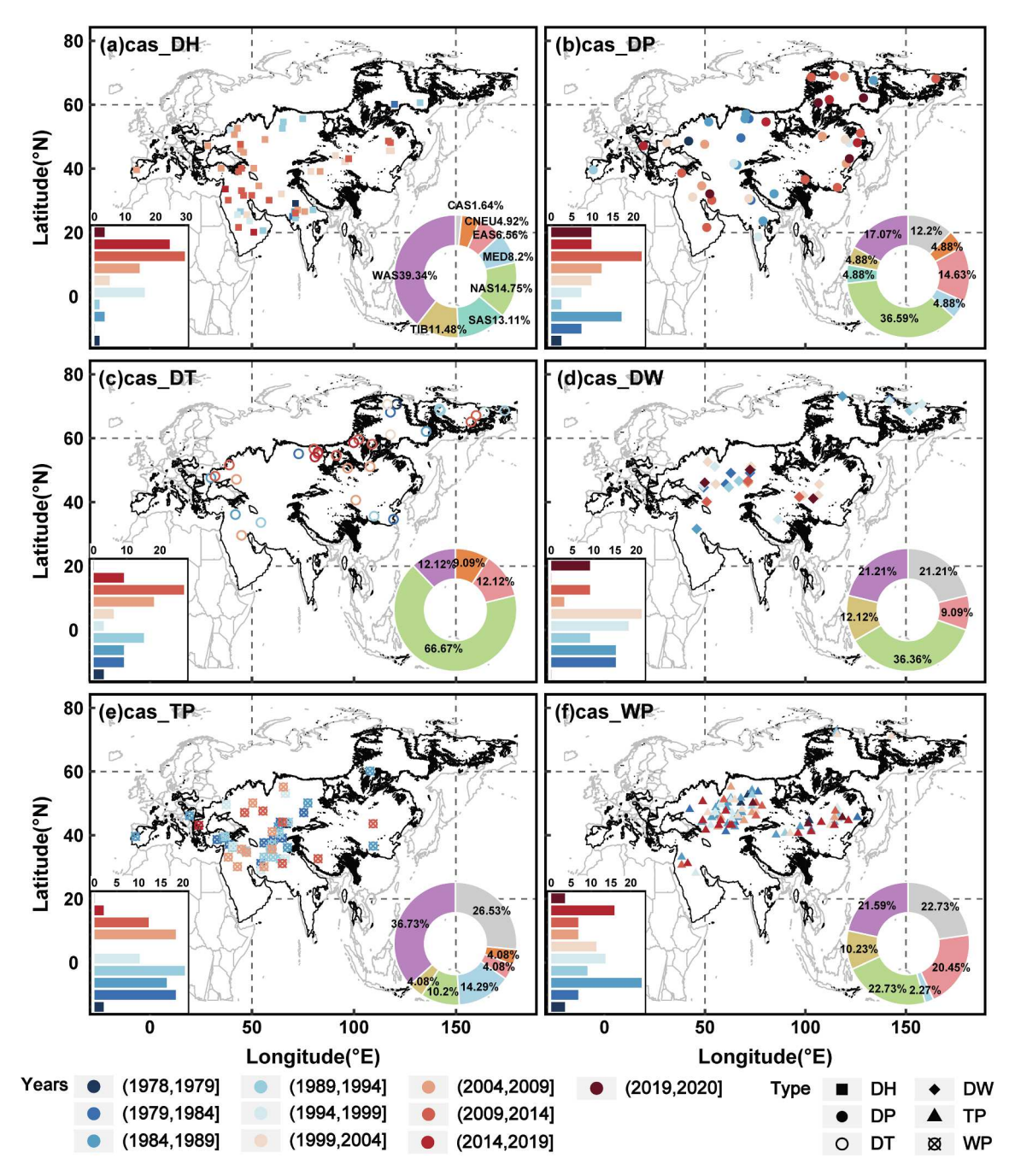


Fig. 11. Temporal and spatial shifting in centroid of typical cas\_CEs.

cas\_CEs are similar, but com\_CEs has a wider geographic and spatial scope, and the cascading extreme has a longer duration. The most typical combination was DH, which is the predominant extreme in summer across the continent, with hotspots in the Arabian Peninsula and the Eastern European Plain. In contrast to DH, DT dominate the types of extreme winter events at high latitudes, accounting for more than 85 % of extreme winter events in this region. However, the hotspots of com\_DT show a southward movement in recent years, which deserves careful observation. DW and WP dominated the types of extreme events in spring and autumn in the mid-latitude region, particularly in Central Asia and the Mongolian Plateau. Finally, although the return periods of com\_DP and cas\_DP are very long on a long-term scale, this may be because DP has only emerged in recent years (mostly after 2000) and is dominant in the summer and autumn. The threat of future extreme events will become greater under the background of climate change,

especially in the mid-latitudes.

In general, recognizing the temporal and spatial patterns of com\_CEs and cas\_CEs and understanding their occurrence patterns and hotspots will help us better prepare for responding to extreme events. Some key research questions need to be included in future studies: (1) The traditional percentile-based algorithm provides a time- and labor-saving method for the analysis of extreme events. However, studies in large regions, especially when there is a large difference between regions, require the auxiliary judgment of a shared global database of extreme event records. (2) More effort needs to be put into exploring changes in the risk of extreme event combinations in the mid-latitudes of Eurasia, especially the devastating consequences of hyperactive extreme events on regional ecosystems.

#### CRediT authorship contribution statement

Huiqian Yu: Conceptualization, Software. Nan Lu: Supervision. Bojie Fu: Funding acquisition. Lu Zhang: . Mengyu Wang: . Hanqin Tian: Funding acquisition.

## **Declaration of Competing Interest**

The authors declare that they have no known competing financial interests or personal relationships that could have appeared to influence the work reported in this paper.

#### Data availability

The data and code used in this manuscript is open access. And relevant links have been attached in the Section 2 Data and Methods.

#### Acknowledgement

Thanks are due to Yuedan Zhao for proof reading the article.

#### Funding

This work is supported by National Natural Science Foundation of China (NSFC) (41991234), Joint CAS-MPG Research Project HZXM20225001MI, the National Science Foundation (1903722) and Andrew Carnegie Fellowship Program (G-F-19-56910).

## Appendix A. Supplementary material

Supplementary data to this article can be found online at https://doi.org/10.1016/j.envint.2022.107509.

## References

- Ahlström, A., Raupach, M.R., Schurgers, G., et al., 2015. The dominant role of semi-arid ecosystems in the trend and variability of the land CO2 sink. Science 348 (6237), 895–899.
- Alexander, L.V., Zhang, X., Peterson, T.C., et al., 2006. Global observed changes in daily climate extremes of temperature and precipitation. J. Geophys. Res. 111, D05109. Barriopedro, D., Fischer, E., Luterbacher, J., et al., 2011. The hot summer of 2010:
- redrawing the temperature record map of Europe. Science 332, 220–224.
- Bastos, A., Fu, Z., Ciais, P., et al., 2020a. Impacts of extreme summers on European ecosystems: a comparative analysis of 2003, 2010 and 2018. Philos. Trans. Roy. Soc. B Biol. Sci. 375(1810), 20190507.
- Bastos, A., Ciais, P., Friedlingstein, P., et al., 2020b. Direct and seasonal legacy effects of the 2018 heat wave and drought on European ecosystem productivity. Sci. Adv. 6 (24), eaba2724.
- Berdugo, M., Delgado-Baquerizo, M., Soliveres, S., et al., 2020. Global ecosystem thresholds driven by aridity. Science 367 (6479), 787–790.
- Birant, D., Kut, A., 2007. ST-DBSCAN: An algorithm for clustering spatial-temporal data. Data Knowl. Eng. 60 (1), 208–221.
- Cai, L., Li, Y., Chen, M., et al., 2020. Tropical cyclone risk assessment for China at the provincial level based on clustering analysis. Geomat. Nat. Hazards Risk 11 (1), 869–886.
- Chen, L., Francis, J., Hanna, E., 2018. The "Warm-Arctic/Cold-continents" pattern during 1901–2010. Int. J. Climatol. 38 (14), 5245–5254.
- Cohen, J., Screen, J.A., Furtado, J.C., et al., 2014. Recent Arctic amplification and extreme mid-latitude weather. Nat. Geosci. 7 (9), 627–637.
- Coumou, D., Rahmstorf, S., 2012. A decade of weather extremes. Nat. Clim. Change 2 (7), 491–496.
- Coumou, D., Petoukhov, V., Rahmstorf, S., et al., 2014. Quasi-resonant circulation regimes and hemispheric synchronization of extreme weather in boreal summer. PNAS 111 (34), 12331–12336.
- Di Martino, F., Pedrycz, W., Sessa, S., 2018. Spatiotemporal extended fuzzy C-means clustering algorithm for hotspots detection and prediction. Fuzzy Sets Syst. 340, 109–126.
- Diffenbaugh, N.S., Pal, J.S., Giorgi, F., et al., 2007. Heat stress intensification in the Mediterranean climate change hotspot. Geophys. Res. Lett. 34 (11), L11706.
- Donat, M.G., Alexander, L.V., Yang, H., et al., 2013a. Global land-based datasets for monitoring climatic extremes. Bull. Am. Meteorol. Soc. 94 (7), 997–1006.
- Donat, M.G., Alexander, L.V., Yang, H., et al., 2013b. Updated analyses of temperature and precipitation extreme indices since the beginning of the twentieth century: the HadEX2 dataset. J. Geophys. Res.: Atmos. 118 (5), 2098–2118.

- Feng, S., Hao, Z., Zhang, X., et al., 2019. Probabilistic evaluation of the impact of compound dry-hot events on global maize yields. Sci. Total Environ. 689, 1228–1234.
- Francis, J.A., Vavrus, S.J., 2015. Evidence for a wavier jet stream in response to rapid Arctic warming. Environ. Res. Lett. 10 (1), 014005.
- Fraser, E.D.G., Dougill, A.J., Hubacek, K., et al., 2011. Assessing vulnerability to climate change in dryland livelihood systems: conceptual challenges and interdisciplinary solutions. Ecol. Soc. 16 (3), 3. https://doi.org/10.5751/ES-03402-160303.
- Frierson, D.M.W., Scheff, J., 2015. Terrestrial aridity and its response to greenhouse warming across CMIP5 climate models. J. Clim. 28 (14), 5583–5600.
- Fu, Q., Feng, S., 2014. Responses of terrestrial aridity to global warming. J. Geophys. Re.: Atmos. 119 (13), 7863–7875.
- Gao, Y., Zhang, J., Yan, F., et al., 2020. Nonlinear effect of compound extreme weather events on ozone formation over the United States. Weather Clim. Extremes 30, 100285.
- García-Herrera, R., Díaz, J., Trigo, R.M., et al., 2010. A review of the European summer heat wave of 2003. Crit. Rev. Environ. Sci. Technol. 40 (4), 267–306.
- Grumm, R.H., 2011. The central European and Russian Heat event of July–August 2010. Bull. Am. Meteorol. Soc. 92 (10), 1285–1296.
- Hao, Z., Hao, F., Singh, V.P., et al., 2018. Changes in the severity of compound drought and hot extremes over global land areas. Environ. Res. Lett. 13 (12), 124022.
- Hao, Y., Hao, Z., Fu, Y., et al., 2021. Probabilistic assessments of the impacts of compound dry and hot events on global vegetation during growing seasons. Environ. Res. Lett. 16 (7), 074055.
- Hauser, M., Orth, R., Seneviratne, S.I., 2016. Role of soil moisture versus recent climate change for the 2010 heat wave in western Russia. Geophys. Res. Lett. 43 (6), 2819–2826.
- He, B.-R., Zhai, P.-M., 2018. Changes in persistent and non-persistent extreme precipitation in China from 1961 to 2016. Adv. Clim. Change Res. 9 (3), 177–184.
- Hersbach, H., Bell, B., Berrisford, P., et al. (2019). Global reanalysis: goodbye ERA-Interim, hello ERA5. Meteorology section of ECMWF Newsletter, No. 159, 17-24.
- Hong, C., Hsu, H., Lin, N., et al., 2011. Roles of European blocking and tropicalextratropical interaction in the 2010 Pakistan flooding. Geophys. Res. Lett. 38 (13), L13806.
- Hong, X., Lu, R., Li, S., 2017. Amplified summer warming in Europe-West Asia and Northeast Asia after the mid-1990s. Environ. Res. Lett. 12 (9), 094007.
- Hu, Z., Zhang, C., Hu, Q., et al., 2014. Temperature Changes in Central Asia from 1979 to 2011 Based on Multiple Datasets\*. J. Clim. 27 (3), 1143–1167.
- Huang, W., Kan, H., Kovats, S., 2010. The impact of the 2003 heat wave on mortality in Shanghai, China. Sci. Total Environ. 408 (11), 2418–2420.
- Huang, J., Yu, H., Guan, X., et al., 2015. Accelerated dryland expansion under climate change. Nat. Clim. Change 6 (2), 166–171.
- Hutter, H.P., Moshammer, H., Wallner, P., et al., 2007. Heatwaves in Vienna: effects on mortality. Wien. Klin. Wochenschr. 119 (7–8), 223–227.
- IPCC, 2012. Managing the Risks of Extreme Events and Disasters to Advance Climate Change Adaptation. A Special Report of Working Groups I and II of the Intergovernmental Panel on Climate Change [Field, C.B., V. Barros, T.F. Stocker, D. Qin, D.J. Dokken, K.L. Ebi, M.D. Mastrandrea, K.J. Mach, G.-K. Plattner, S.K. Allen, M. Tignor, and P.M. Midgley (eds.)]. Cambridge University Press, Cambridge, UK, and New York, NY, USA, 582 pp.
- IPCC, 2021. Summary for Policymakers. In: Climate Change 2021: The Physical Science Basis. Contribution of Working Group I to the Sixth Assessment Report of the Intergovernmental Panel on Climate Change. Available at: https://www.ipcc.ch/report/ar6/wg1/downloads/report/IPCC\_AR6\_WG1\_SPM\_final.pdf.
- Johnson, N.C., Xie, S.P., Kosaka, Y., et al., 2018. Increasing occurrence of cold and warm extremes during the recent global warming slowdown. Nat. Commun. 9 (1), 1724.
- Karl, T.R., Nicholls, N., Ghazi, A., 1999. Clivar/GCOS/WMO workshop on indices and indicators for climate extremes workshop summary. Clim. Change 42, 3–7.
- Konapala, G., Mishra, A.K., Wada, Y., et al., 2020. Climate change will affect global water availability through compounding changes in seasonal precipitation and evaporation. Nat. Commun. 11 (1), 3044.
- Konovalov, I.B., Beekmann, M., Kuznetsova, I.N., et al., 2011. Atmospheric impacts of the 2010 Russian wildfires: integrating modelling and measurements of an extreme air pollution episode in the Moscow region. Atmos. Chem. Phys. 11 (19), 10031–10056.
- Kornhuber, K., Petoukhov, V., Petri, S., et al., 2016. Evidence for wave resonance as a key mechanism for generating high-amplitude quasi-stationary waves in boreal summer. Clim. Dyn. 49 (5–6), 1961–1979.
- Kornhuber, K., Osprey, S., Coumou, D., et al., 2019a. Extreme weather events in early summer 2018 connected by a recurrent hemispheric wave-7 pattern. Environ. Res. Lett. 14 (5), 054002.
- Kornhuber, K., Coumou, D., Vogel, E., et al., 2019b. Amplified Rossby waves enhance risk of concurrent heatwaves in major breadbasket regions. Nat. Clim. Change 10 (1), 48–53.
- Koutroulis, A.G., 2019. Dryland changes under different levels of global warming. Sci. Total Environ. 655, 482–511.
- Krzyżewska, A., Dyer, J., 2018. Local-scale analysis of temperature patterns over Poland during heatwave events. Theor. Appl. Climatol. 135 (1–2), 261–277.
- Leonard, M., Westra, S., Phatak, A., et al., 2013. A compound event framework for understanding extreme impacts. WIREs Clim. Change 5 (1), 113–128.
- Lian, X., Piao, S., Chen, A., et al., 2021. Multifaceted characteristics of dryland aridity changes in a warming world. Nat. Rev. Earth Environ. 2 (4) https://doi.org/ 10.1038/s43017-43021-00144-43010.
- Liu, X., He, B., Guo, L., et al., 2020. Similarities and Differences in the Mechanisms Causing the European Summer Heatwaves in 2003, 2010, and 2018. Earth's Future, 7, e2019EF001386.

- Liu, Y., He, J., Yao, S., et al., 2018. An improved St-DBSCAN algorithm based on center of gravity shifting (In Chinese). Comput. Technol. Dev. 28 (11), 6-11.
- Liu, Y., Singleton, A., Arribas-bel, D., et al., 2021b. Identifying and understanding roadconstrained areas of interest (AOIs) through spatiotemporal taxi GPS data: A case study in New York City. Computers, Environment and Urban Systems, p. 86.
- Liu, H., Xu, C., Allen, C.D., et al., 2021a. Nature-based framework for sustainable afforestation in global drylands under changing climate. Glob. Change Biol. 28 (7), 2202-2220.
- Lu, C., Tian, H., Zhang, J., et al., 2019. Severe long-lasting drought accelerated carbon depletion in the Mongolian plateau. Geophys. Res. Lett. 46 (10), 5303-5312.
- Maestre, F.T., Benito, B.M., Berdugo, M., et al., 2021. Biogeography of global drylands. New Phytol. 231 (2), 540-558.
- Mantgem, P. J. v., Stephenson, N. L., Byrne, J. C., et al. (2009). Widespread increase of tree mortality rates in the western United States. Science, 323(5913), 521-524.
- Martius, O., Pfahl, S., Chevalier, C., 2016. A global quantification of compound precipitation and wind extremes. Geophys. Res. Lett. 43 (14), 7709-7717.
- Mazdiyasni, O., AghaKouchak, A., 2015. Substantial increase in concurrent droughts and heatwaves in the United States. PNAS 112 (37), 11484-11489.
- McMichael, A.J., Lindgren, E., 2011. Climate change: present and future risks to health, and necessary responses. J. Intern. Med. 270 (5), 401-413.
- Messori, G., Bevacqua, E., Caballero, R., et al., 2021. Compound climate events and extremes in the Midlatitudes: dynamics, simulation, and statistical characterization. Bull. Am. Meteorol. Soc. 102 (4), E774-E781.
- Miao, L., Ye, P., He, B., et al., 2015. Future climate impact on the desertification in the dry land asia using AVHRR GIMMS NDVI3g Data. Remote Sensing 7 (4), 3863-3877.
- Mishra, A.K., Singh, V.P., 2010. A review of drought concepts. J. Hydrol. 391 (1-2),
- Mori, M., Watanabe, M., Shiogama, H., et al., 2014. Robust Arctic sea-ice influence on the frequent Eurasian cold winters in past decades. Nat. Geosci. 7 (12), 869–873.
- Mori, M., Kosaka, Y., Watanabe, M., et al., 2019. A reconciled estimate of the influence of Arctic sea-ice loss on recent Eurasian cooling. Nat. Clim. Change 9 (2), 123-129.
- Overland, J.E., Wood, K.R., Wang, M., 2011. Warm Arctic-cold continents: climate impacts of the newly open Arctic Sea. Polar Res. 30 (1), 15787.
- Pan, S., Yang, J., Tian, H., et al., 2020. Climate extreme versus carbon extreme: responses of terrestrial carbon fluxes to temperature and precipitation. J. Geophys. Res.: Biogeosci. 125(4), e2019JG005252.
- Pascale, S., Lucarini, V., Feng, X., et al., 2014. Analysis of rainfall seasonality from observations and climate models. Clim. Dyn. 44 (11-12), 3281-3301.
- Pascale, S., Lucarini, V., Feng, X., et al., 2015. Projected changes of rainfall seasonality and dry spells in a high greenhouse gas emissions scenario. Clim. Dyn. 46 (3-4), 1331-1350.
- Peng, C., Ma, Z., Lei, X., et al., 2011. A drought-induced pervasive increase in tree mortality across Canada's boreal forests. Nat. Clim. Change 1 (9), 467–471.
- Perkins-Kirkpatrick, S.E., Lewis, S.C., 2020. Increasing trends in regional heatwaves. Nat. Commun. 11 (1), 3357.
- Pescaroli, G., Alexander, D., 2015. A definition of cascading disasters and cascading effects: Going beyond the "toppling dominos" metaphor. Global Forum Davos 2 (3), 58-67
- Peterson, T.C., 2005. Climate Change Indices. WMO Bulletin 54 (2), 83–86.
  Peterson, T. C., Folland, C., Gruza, G., et al., 2001. Report on the Activities of the Working Group on Climate Change Detection and Related Rapporteurs 1998-2001. WMO, Rep. WCDMP-47, WMO-TD 1071, Geneve, Switzerland, 143pp.
- Petoukhov, V., Semenov, V.A., 2010. A link between reduced Barents-Kara sea ice and cold winter extremes over northern continents. J. Geophys. Res. 115 (D21), D21111.
- Phillips, O.L., Aragao, L.E., Lewis, S.L., et al., 2009. Drought sensitivity of the Amazon rainforest. Science 323 (5919), 1344–1347.
- Piao, S., Wang, X., Wang, K., et al., 2020. Interannual variation of terrestrial carbon cycle: issues and perspectives. Glob. Change Biol. 26 (1), 300-318.
- Poulter, B., Frank, D., Ciais, P., et al., 2014. Contribution of semi-arid ecosystems to interannual variability of the global carbon cycle. Nature 509 (7502), 600-603.
- Raveh-Rubin, S., Wernli, H., 2015. Large-scale wind and precipitation extremes in the Mediterranean: a climatological analysis for 1979-2012. Q. J. R. Meteorolog. Soc. 141 (691), 2404-2417.
- Ray, K., Giri, R.K., Ray, S.S., et al., 2021. An assessment of long-term changes in mortalities due to extreme weather events in India: a study of 50 years' data, 1970-2019. Weather Clim. Extremes 32, 100315.
- Ribeiro, A.F.S., Russo, A., Gouveia, C.M., et al., 2020. Risk of crop failure due to compound dry and hot extremes estimated with nested copulas. Biogeosciences 17 (19), 4815-4830.
- Ridder, N.N., Pitman, A.J., Westra, S., et al., 2020. Global hotspots for the occurrence of compound events. Nat. Commun. 11 (1), 5956.
- Robine, J.M., Cheung, S.L., Le Roy, S., et al., 2008. Death toll exceeded 70,000 in Europe during the summer of 2003. C.R. Biol. 331 (2), 171-178.
- Röthlisberger, M., Martius, O., 2019. Quantifying the local effect of northern hemisphere atmospheric blocks on the persistence of summer hot and dry spells. Geophys. Res. Lett. 46 (16), 10101-10111.

- Russo, S., Dosio, A., Graversen, R.G., et al., 2014. Magnitude of extreme heat waves in present climate and their projection in a warming world. J. Geophys. Res.: Atmos. 119 (22) https://doi.org/10.1002/2014JD022098.
- Sarhadi, A., Ausín, M.C., Wiper, M.P., et al., 2018. Multidimensional risk in a nonstationary climate: joint probability of increasingly severe warm and dry conditions. Sci. Adv. 4, eaau3487.
- Schlaepfer, D.R., Bradford, J.B., Lauenroth, W.K., et al., 2017. Climate change reduces extent of temperate drylands and intensifies drought in deep soils. Nat. Commun. 8,
- Schumacher, D.L., Keune, J., van Heerwaarden, C.C., et al., 2019. Amplification of megaheatwaves through heat torrents fuelled by upwind drought. Nat. Geosci. 12 (9), 712-717.
- Screen, J.A., Simmonds, I., 2014. Amplified mid-latitude planetary waves favour particular regional weather extremes. Nat. Clim. Change 4 (8), 704-709.
- Shaposhnikov, D., Revich, B., Bellander, T., et al., 2014. Mortality related to air pollution with the Moscow heat wave and wildfire of 2010. Epidemiology 25 (3), 359-364.
- Sharma, S., Mujumdar, P., 2017. Increasing frequency and spatial extent of concurrent meteorological droughts and heatwaves in India. Sci. Rep. 7 (1), 15582.
- Sitanggang, I.S., Radiatun, N., Nur Risal, A.A., 2020. Incremental Spatio temporal clustering application on hotspot data. IOP Conf. Series: Earth Environ. Sci. 528 (1),
- Sivakumar, M.V.K., 2007. Interactions between climate and desertification. Agric. For. Meteorol. 142 (2-4), 143-155.
- Stefanon, M., D'Andrea, F., Drobinski, P., 2012. Heatwave classification over Europe and the Mediterranean region. Environ. Res. Lett. 7 (1), 014023.
- Sun, X., Sun, Q., Zhou, X., et al., 2014. Heat wave impact on mortality in Pudong New Area, China in 2013. Sci. Total Environ. 493, 789-794.
- Sutanto, S.J., Vitolo, C., Di Napoli, C., et al., 2020. Heatwaves, droughts, and fires: Exploring compound and cascading dry hazards at the pan-European scale. Environ. Int. 134, 105276.
- Tang, Q., Zhang, X., Yang, X., et al., 2013. Cold winter extremes in northern continents linked to Arctic sea ice loss. Environ. Res. Lett. 8 (1), 014036.
- Tao, S., Fang, J., Zhao, X., et al., 2015. Rapid loss of lakes on the Mongolian Plateau. PNAS 112 (7), 2281-2286.
- Telesca, L., Guignard, F., Laib, M., et al., 2020. Analysis of temporal properties of extremes of wind measurements from 132 stations over Switzerland. Renew. Energy 145, 1091-1103.
- Tian, H., Lu, C., Chen, G., et al., 2011. Climate and land use controls over terrestrial water use efficiency in monsoon Asia. Ecohydrology 4 (2), 322-340.
- Vitolo, C., Di Napoli, C., Di Giuseppe, F., et al., 2019. Mapping combined wildfire and heat stress hazards to improve evidence-based decision making. Environ. Int. 127, 21-34.
- Vogel, J., Paton, E., Aich, V., et al., 2021. Increasing compound warm spells and droughts in the Mediterranean Basin. Weather Clim. Extremes 32, 100312.
- Wang, J., Chen, Y., Tett, S.F.B., et al., 2020a, Anthropogenically-driven increases in the risks of summertime compound hot extremes. Nat. Commun. 11 (1), 528.
- Wang, S.-Y., Davies, R.E., Gillies, R.R., 2013. Identification of extreme precipitation threat across midlatitude regions based on short-wave circulations, J. Geophys, Res.: Atmos. 118 (19), 11059-11074.
- Wang, Z., Yao, M., Meng, C., et al., 2020b. Risk assessment of the overseas imported COVID-19 of ocean-going ships based on AIS and infection data. ISPRS Int. J. Geo-Inf. 9 (6).
- Witte, J.C., Douglass, A.R., da Silva, A., et al., 2011. NASA A-Train and Terra observations of the 2010 Russian wildfires. Atmos. Chem. Phys. 11 (17), 9287-9301.
- WMO, 2012, Is it Now Possible to Blame Extreme Weather on Global Warming? Bulletin of the World Meteorological Organization, 61(2), Available at: https://public.wmo.int/ en/resources/bulletin/it-now-possible-blame-extreme-weather-global-warming.
- Xu, Z., FitzGerald, G., Guo, Y., et al., 2016. Impact of heatwave on mortality under different heatwave definitions: a systematic review and meta-analysis. Environ. Int. 89-90, 193-203.
- Yao, J., Liu, H., Huang, J., et al., 2020. Accelerated dryland expansion regulates future variability in dryland gross primary production. Nat. Commun. 11 (1), 1665.
- Ye, K., Messori, G., 2020. Two leading modes of wintertime atmospheric circulation drive the recent warm arctic-cold eurasia temperature pattern. J. Clim. 33 (13), 5565-5587
- Yu, L., Zhong, S., 2019. Strong wind speed events over Antarctica and its surrounding oceans. J. Clim. 32 (12), 3451-3470.
- Zhang, J., Gao, Y., Luo, K., et al., 2018. Impacts of compound extreme weather events on ozone in the present and future. Atmos. Chem. Phys. 18 (13), 9861-9877.
- Zhang, Y., Sun, X., Chen, C., 2021. Characteristics of concurrent precipitation and wind speed extremes in China. Weather Clim. Extremes 32, 100322.
- Zscheischler, J., Westra, S., van den Hurk, B.J.J.M., et al., 2018. Future climate risk from compound events. Nat. Clim. Change 8 (6), 469-477.